Unveiling the prehistoric landscape at Stonehenge through multi-receiver EMI

Philippe De Smedt*[1], Marc Van Meirvenne[1], Timothy Saey[1], Eamonn Baldwin[2], Chris Gaffney[3], Vince Gaffney[2]

[1]*Research Group Soil Spatial Inventory Techniques, Department of Soil Management, Ghent University, Coupure 653, 9000 Ghent, Belgium*

[2] *Department of Classics, Ancient History and Archaeology/Hub for Digital Humanities, University of Birmingham, Edgbaston, Birmingham B15 2TT, UK*

[3] *Archaeological Sciences, School of Applied Sciences, University of Bradford, Bradford, West Yorkshire, BD7 1DP, UK*

*Corresponding author: Fax: +3292646247

Tel: +3292646042

Mail: Philippe.DeSmedt@UGent.be

Abstract

Archaeological research at Stonehenge (UK) is increasingly aimed at understanding the dynamic of the wider archaeological landscape. Through the application of state-of-the-art geophysical techniques, unprecedented insight is being gathered into the buried archaeological features of the area. However, applied survey techniques have rarely targeted natural soil variation, and the detailed knowledge of the palaeotopography is consequently less complete. In addition, metallic topsoil debris, scattered over different parts of the Stonehenge landscape, often impacts the interpretation of geophysical datasets. The research presented here demonstrates how a single multi-receiver electromagnetic induction (EMI) survey, conducted over a 22 ha area within the Stonehenge landscape, offers detailed insight into natural and anthropogenic soil variation at Stonehenge. The soil variations that were detected through recording the electrical and magnetic soil variability, shed light on the genesis of the landscape, and allow for a better definition of potential palaeoenvironmental and archaeological sampling locations. Based on the multi-layered dataset, a procedure was developed to remove the influence of topsoil metal from the survey data, which enabled a more straightforward identification of the detected archaeology. The results provide a robust basis for further geoarchaeological research, while potential to differentiate between modern soil disturbances and the underlying sub-surface variations can help in solving conservation and management issues. Through expanding this approach over the wider area, we aim at a fuller understanding of the human-landscape interactions that have shaped the Stonehenge landscape.

1. Introduction

The archaeological landscape of the Stonehenge (UK) results from at least 12 000 years of human occupation, during which prehistoric societies transformed the area into a ritual landscape. An abundance of prehistoric monuments, with the standing stone monument as the most iconic example, are distributed over approximately 25 km^2 and are witness to such prehistoric human-landscape interactions. Human action continues to influence this archaeological complex, with notable examples including the militarisation of the wider area starting in the end of the 19^{th} century, along with conservation and management measures, and the designation of Stonehenge as a UNESCO World Heritage Site (WHS) (ICOMOS, 1986).

Stonehenge has attracted research interest from scholars over centuries (Darvill, 2006) and this has made it one of the most investigated archaeological landscapes in the world. Whereas the individual monuments have been the focal point of most early research at the site, landscape archaeological approaches and current research perspectives, such as those set out in the Archaeological Research Framework (Darvill et al., 2005), emphasise the geography and archaeology of the wider area. In line with the status of Stonehenge as a World Heritage Site, this has stimulated a non-invasive approach, and geophysical and remote sensing methods are increasingly being applied to tackle current gaps in knowledge concerning the archaeological landscape. The most recent in a series of research projects is the *Stonehenge Hidden Landscapes Project* (SHLP), which aims to study the archaeological landscape, rather than the individual monuments (Gaffney et al., 2012).

Along with other non-invasive mapping using, for example, Light Detection and Ranging (LiDAR) (Bewley et al., 2005; Crutchley, 2002), extensive geophysical surveying significantly enhances our archaeological insight into the Stonehenge landscape (Underhill, 2011). Understanding the detailed pedological variations in the area, however, is less developed. Geological surveys (e.g. Hopson et al., 2006) have characterized the general stratigraphy of the Salisbury Plain, and soil micromorphological analyses have have supported the identification of prehistoric soil profiles (Macphail and Crowther, 2008). Past research campaigns have already recognized the importance of soil survey at Stonehenge, as some of these have focussed on the detection of colluvial deposits that potentially seal archaeological features and contain palaeoenvironmental information (Richards, 1990). However,

to date only a limited number of depositional environments in the area have been detected and made available for study (Leivers and Moore, 2008).

The geology of the Stonehenge landscape consists of Upper Chalk covered with calcareous drift deposits, loess and occasional clay-with-flint patches (Canti et al., 2013; Richards, 1990). On top of these sediments the most widely present soil types are rendzinas, and silty soils with occasional clay enrichment (argillic brown earths and brown calcareous earths (Richards, 1990)). In these well drained soils the preservation of sealed or waterlogged deposits is scarce (French, 2003), and within WHS the soil depth is generally limited. This makes locating colluvial deposits and deeper soil profiles a methodological challenge, but essential to further understanding of the prehistoric Stonehenge environment.

The more recent land-use at Stonehenge poses a specific set of problems when working with geophysical survey data from the site. In large areas of the landscape, military activities, mainly dating to the first half of the twentieth century, have significantly disturbed the soil. From firing ranges to the Stonehenge Down airfield south east of Stonehenge, these activities have left behind a large amount of metal debris in the soil that can 'pollute' geophysical data (Darvill et al., 2013; Gaffney et al., 2012). Additional magnetic material left behind during music festivals that took place in the 1970's and -80's, further contributes to such noise in geophysical data (Darvill et al., 2013).

To respond to these site-specific issues, we propose to carry out area-wide multi-receiver electromagnetic induction (EMI) survey across of the Stonehenge landscape. While small scale tests with EMI instruments have been conducted over individual monuments at Stonehenge (Bonsall et al., 2013; Gaffney et al., 2012), large-area EMI survey has not yet been taken undertaken. Through advances in soil science and proximal soil sensing (Rossel et al., 2010), EMI sensors have become a very effective tool for mapping soil variation by recording the soil apparent electrical conductivity (σ_a) (Corwin and Lesch, 2005; Rhoades et al., 1976; Sudduth et al., 2005). The strong relationship between σ_a and soil texture is of particular interest as it allows the creation of detailed soil maps based on EMI data (Saey et al., 2009a). At Stonehenge, this use of geophysical soil mapping can help provide the detailed information needed to reconstruct the palaeotopography of the area, and pinpoint both palaeoenvironmental and archaeological sampling locations.

Whereas the main geophysical survey techniques that are used in archaeology (magnetometry, electrical resistivity and ground penetrating radar (GPR)) each target only one specific variable, EMI offers the potential to measure both σ_a and apparent magnetic susceptibility (κ_a) simultaneously. This combined registration of different physical soil variables allows broad insight into the anthropogenic and natural soil variations, thus facilitating an integral geoarchaeological reconstruction (e.g. De Smedt et al., 2013a). Multi-receiver EMI soil sensors further add the potential to discriminate changes in σ_a and κ_a in three dimensions by simultaneously measuring multiple soil volumes (Saey et al., 2009b). This has already enabled the visualization of vertical σ_a-variations to reconstruct past landforms (De Smedt et al., 2013b; Saey et al., 2008) and past human environments (De Smedt et al., 2013c).

In September 2012, a multi-receiver EMI survey was undertaken to evaluate the technique's potential for mapping anthropogenic and natural subsurface variations within the Stonehenge landscape. An area of 22 ha was selected near the western extent of the Stonehenge Cursus, where in the 1970s and 1980s camps were positioned for Stonehenge Free music festival (Fig. 1). The magnetic debris from these festivals leaves magnetometry data plots peppered with small metallic anomalies that limit the archaeological interpretation of the images (Darvill et al., 2013; Gaffney et al., 2012). While the use of a multi-receiver instrument offers insight into the lateral and vertical soil variability, we further examined how the multi-layered EMI dataset can aid in discriminating between recent topsoil debris and the underlying archaeology. The presented research forms the start of a large-scale EMI mapping programme at Stonehenge, whereby a core area of 2.5 km^2 will be surveyed with multi-receiver EMI over the course of the next three years. In this paper, we present the first survey results with particular focus on the soil variation and the potential to discriminate recent disturbances from the underlying archaeology in the study area.

2. Multi-receiver electromagnetic induction

2.1 Instrumentation

We used a multi-receiver EMI instrument that combines one transmitter coil with four receiver coils that simultaneously record the soil σ_a and κ_a (Dualem-21S, Dualem, Canada). The receiver coils are placed in two orientations (horizontal coplanar (HCP) and perpendicular (PRP)) at both 1 m and 2 m

from the transmitter (Simpson et al., 2009). Through using different coil orientations with the same intercoil separation different parts of the medium under study can be targeted. When measuring the soil σ_a, a PRP coil configuration with an intercoil separation of 1 m, will obtain most influence from the upper 30 cm of the measured medium. On the other hand, measuring σ_a with a HCP coil pair with the same intercoil separation, the upper part of the medium will affect the recorded signal response in a different manner (McNeill, 1980; Wait, 1962).

While the coil orientation mainly influences the shape of the soil volume that is taken into account, the separation between transmitter and receiver coil influences the size of the measured soil volume. For σ_a, a HCP coil pair with a 1 m intercoil separation has a depth of investigation (DOI, defined as the 70% response depth) of 1.5 m, an intercoil separation of 2 m increases the DOI of such a coil pair down to 3.2 m below the sensor (Saey et al. 2009b). The depth response of the EMI signal differs for the quadrature-phase signal response (representative for the σ_a) and the in-phase signal response (proportional to the soil κ_a), resulting in κ_a data that representative for a differently shaped soil volume than σ_a data of the same coil pair (De Smedt et al., 2014; Simpson et al., 2010). Furthermore, in most field conditions the κ_a data from PRP coil pairs suffer from high-frequency noise, making them difficult to interpret (De Smedt et al., 2014). For this reason, the PRP κ_a data have not been used in this study. The EMI survey thus results in a six-layered dataset where the maximum depth penetration of the σ_a measurements reaches 3.2 m below the sensor, while the HCP κ_a measurements have maximum depth response of approximately 1.5 m below the sensor.

2.2 Survey strategy and data processing

The study area (Fig. 1) was surveyed between the 17th and 21st of September 2012, using a mobile configuration, whereby the EMI sensor was towed behind a quad bike. The use of a differential GPS (dGPS) with an accuracy ≤ 10 cm allowed for real-time georeferencing, and for the registration of the terrain elevation. EMI measurements were taken along parallel lines, 1.2 m apart and driven in alternating directions, with one sampling cycle every 0.25 m. With this sampling resolution larger archaeological features were targeted, along with the small-scale pedological and geomorphological variations. Each day, soil temperature was recorded at 30 cm below the surface to account for temperature differences in the σ_a data between survey days (Slavich and Petterson, 1990). Before every survey, a calibration line was driven across the area to correct for potential measurement drift

following Simpson et al. (2009). In a final step, ordinary kriging (Goovaerts, 1997) was performed to interpolate the survey data to 0.1 m by 0.1 m raster images.

3 Survey results

3.1 Filtering out metallic topsoil debris

As in published magnetometry datasets from the area (Darvill et al., 2013; Gaffney et al., 2012), a large amount of local spatial data outliers occur in the EMI data, which are mainly caused by magnetic debris related to the refuse left behind during the 1970s-80s music festivals (Fig. 2a). The objects causing such anomalies are primarily located in the topsoil, producing a widespread and identifiable signature in the in the EMI data. Their influence on the measurements from the four coil configurations, however, differs significantly. In Fig. 3 the EMI measurements are compared for one of the outliers. Note how the anomaly influences coil pairs with 1 m and 2 m intercoil separation differently. Whereas the anomaly is strongly present in the 1 m PRP and HCP σ_a data (Fig. 3a, c), its influence is negligible in the 2 m PRP and HCP data (Fig. 3c). For the κ_a data, the same effect can be seen (Fig. 3d). However, while such an anomaly causes extreme values in the σ_a data (e.g. strongly negative in the 1 m HCP σ_a data (Fig. 2 and 3), these represent local spatial outliers in the κ_a data, which are often situated within the normal measurement range. As features that have been cut into the soil (e.g. pits) have the same spatial extent as the metal-induced anomalies, the use of spatial filters to reduce outlier influence such as median filtering (Scollar et al., 1990) carries the risk of removing archaeological data from the measurements.

Fig. 2 near here

Fig. 3 near here

To reduce the influence of topsoil metal on the κ_a data, the location of the metal anomalies was therefore deduced from the σ_a data. In the 1m HCP σ_a data layer, the influence of the topsoil debris is the most prominent, resulting in a strongly negative signal response (Fig. 3a, c). Near larger metal objects, strongly positive σ_a values were recorded. Within the low conductive environment at Stonehenge, the high σ_a values can be identified as the upper 1% percentile of the 1HCP σ_a data values (i.e. above 9.2 mS/m, ranging up to 312.3 mS/m). By extracting these data points along with

negative data from the 1 m HCP σ_a measurements, a map of the metal scatter was produced (Fig. 2b). With this information, the influence from the metallic topsoil contamination was removed from the κ_a data layers by discarding the measurements made on the identified locations. To account for the different spatial sensitivity from the 2 m HCP coil pair, rendering a wider influence of the detected metallic anomalies, a filter buffer of 1 m was taken into account around the identified metal objects (Fig. 4). To diminish the metal effect on the σ_a data, the same procedure was applied to the σ_a data layers. The presented data in the following sections have all been filtered following this procedure, and were subsequently interpolated to 0.1 by 0.1 m rasters through ordinary kriging (Goovaerts, 1997). The resulting data plots offered a more straightforward insight into the archaeological and natural subsoil variations, and allowed a clearer visualization of the detected archaeological features. As an example, Fig. 5 compares the 2 m HCP κ_a data from a hengiform monument, detected through the SHLP (Gaffney et al., 2012) before and after metal removal. The filtered data (Fig. 5b) allow a straightforward delineation of the different parts of the monument as the shape of the large circle of pits is more clearly defined (see for example the influence of the outliers indicated by arrow 1 on Fig. 5a). Near the south-western entrance of the monument, another large anomaly was identified as a metal-induced outlier (Fig. 5a, arrow 2). On the west of the monument, a group of anomalies remained present in the filtered dataset, indicating a possible archaeological origin (Fig. 5b). (For comparative purposes, all σ_a and κ_a data sets have been made available in pdf-format as online supplementary data.)

Fig. 4 near here

Fig. 5 near here

3.2 Natural soil variation and modern soil disturbance

The natural subsurface variations are most clearly visible in the 2 m PRP σ_a data, representing a soil volume between 0 m – 1 m below the sensor, indicating that most variability is situated within this depth range. As σ_a informs mainly on soil texture (Saey et al. 2009a), the variations seen here can be attributed to the depth of the shallow chalk bedrock, visible as resistive zones, and the overlying more conductive silty soil. Where soil thickness increases, a higher σ_a is attested. Most prominent is the broad band of low σ_a values running east-west through the area, indicating a shallow chalk ridge (A on Fig. 6a). In the south, low σ_a values also show shallow bedrock, but here an irregular pattern of high

and low conductivities further indicates chalk weathering patterns and the infilling of cracks and depressions in the chalk bedrock with more conductive soil. In addition to the large-scale variability, two circular anomalies were detected inside the Cursus (B on Fig. 6a). These were identified as the subsurface expression of naturally formed rings of grassland fungi ('fairy rings') resulting in a detectable increase in soil organic matter content or aggregate formation.

Fig. 6 near here

The chalk morphology and soil variation have almost no influence in the κ_a data. However, in the south of the study area, a band of increased magnetic susceptibility indicates magnetic sediments that are likely related to accumulated organic matter (C on Fig. 6b). The topographical position of this anomaly points to a fluvial origin, suggesting that these sediments are organic enriched palaeochannel infillings.

The κ_a data further show the impact of modern land-use on the preservation of the Stonehenge heritage. Numerous lines run in an east-west and north-south direction through the area, some of which were already located through Ordnance Survey maps and historical aerial photography (Amadio and Bishop, 2010), and most likely testify of former ploughing and field drains. These mainly seem to affect the subsurface archaeology as the lines do not cross the monuments that remain present above ground level.

3.3 Archaeology

Anomalies indicating archaeological features are attested in both the σ_a and κ_a data, and can be discerned the clearest in the 1 m PRP σ_a and 2 m HCP κ_a measurements (Fig. 7). Features that are most apparent in the σ_a data include the Cursus ditch in the north of the site, and the annular anomalies related to known crop marks and barrow monuments (Crutchley, 2002; Gaffney et al., 2012). In the south of the survey area, a number of small conductive anomalies of unknown origin were detected. However, for some their location suggests a correlation to known monuments (see below). Within the boundaries of the Cursus, strongly conductive anomalies indicate pits and linear features (Fig. 6a, Fig. 7a B), a number of which were attested in previous geophysical surveys (Darvill et al., 2013; Gaffney et al., 2012).

Fig. 7 near here

The soil perturbations inside the Cursus are clearly visible in the κ_a data, where apart from the various pit-like anomalies (Fig. 6b, Fig. 7b C), the linear traces show as non-magnetic anomalies (Fig. 6b, Fig. 7b C). Overall, the κ_a data allow for the most straightforward interpretation of the archaeological variations within the area. The 2 m HCP κ_a data allow the clearest delineation of the detected anomalies. As an example we present the hengiform monument that was detected at monument Amesbury 50 (Fig. 5, Fig. 7b F) (Gaffney et al., 2012). Even with the rather coarse sampling density, the interior structure of the feature can be discerned. Traces of at least one ring of pits can be identified, encircled by a large segmented ditch. Additional variation was detected in the centre of the feature, but further analysis of this variation requires a denser sampling resolution. Throughout the area, the known barrow monuments are clearly defined in the κ_a data. For some, the internal structure becomes apparent, along with smaller features surrounding the monuments. Examples include three small magnetic anomalies around the central barrow (known as Amesbury 49) (Fig. 7b E), and the magnetic anomaly in the middle of the circular barrow ditch.

Between the two southernmost barrows two large magnetic anomalies can be seen in alignment with these monuments (Fig. 7b G). As the anomalies occur in several of the EMI datasets (e.g. 1 m HCP σ_a (Fig. 2 a), 1 m HCP κ_a (Fig. 6 b)), these could indicate severely ploughed-out barrows. This hypothesis is supported by the intersection of the westernmost anomaly by one of the linear soil disturbances, which shows that the anomaly predates this modern soil feature.

In the south of the study area, a segmented ditch, known as Amesbury 115, shows up as a concentration of highly susceptible anomalies (Fig. 7c). This annular feature, which has been identified in the 1940s through aerial photography (Amadio and Bishop, 2010), can be seen in the κ_a data as a six-segment causewayed ditch.

4 Discussion

4.1 Discriminating recent soil alterations and metal removal

The procedure to remove the signal produced by topsoil metal from the EMI datasets presented here, offers a straightforward means to discriminate between recent metallic topsoil debris and underlying soil variability. This method provides a solution in areas where similar metallic debris is present in the

topsoil from recent activities (see for example the issue of metal contamination in green waste compost raised by former UK environment minister Benyon (Quinault, 2012)), which are often deemed unsuited for geophysical prospecting due to the large amount of metallic anomalies. At Stonehenge, the resulting map of the metallic anomalies can be used to improve the discrimination of targeted features in the magnetometry datasets that are already available (Darvill et al., 2013; Gaffney et al., 2012). Through combining the topsoil metal locations with the linear modern soil intrusions that were attested throughout the entire survey area, a map can be produced of the modern subsurface disturbances (Fig. 8). Such information can then be used in solving site management and conservation issues.

Fig. 8 near here

4.2 Geoarchaeological soil variation

The combined analysis of current elevation and the natural soil variation of the study area (Fig. 9a), indicates a palaeotopography that differs from the current relief. The central shallow chalk ridge, bordered in the north and south by thicker layers of silty soil overlying the chalk bedrock, is a witness to the erosion of overlying silty soil. In the south of the site, the chalk again becomes more dominant as the steep southern slope boosts soil erosion. At the bottom of this hillside, the palaeochannel segment further indicates past transportation of runoff and eroded sediments towards the east. This southern part of the study area is a potential sampling location for deposits harbouring palaeoenvironmental information. However, coring would be required to verify the hypothesis and determine the detailed stratigraphy of the feature.

Fig. 9 near here

Adding the detected archaeological variation to the soil map allows a preliminary overview of the geoarchaeological soil variation (Fig. 9b). The most prominently situated features within the area are the central barrows (Amesbury 48 and 49; A and B on Fig. 9b), with two possible ploughed-out barrow monuments (Fig. 9b C) aligned between them, following the central chalk ridge and the current topography. The presence of ploughed-out barrows at these locations is further supported by the slight elevation that was attested at the location of each anomaly. In addition, the existence of one such

feature has already been suggested through the Stonehenge WHS Landscape Project (Amadio and Bishop, 2010).

The Cursus ditches and associated banks are recurrent features throughout the EMI data layers (D on Fig 9b). Through reducing the influence of metal in the EMI survey data, a better distinction could be made between the topsoil noise and anomalies indicating past soil intrusions (pits). The location of the most characteristic of these pits is shown in Fig. 9b (E). The linear anomalies within the Cursus boundaries (F on Fig. 9) seem to be associated with some of the detected pits and intersect the Cursus bank. However, the origin of these features remains unknown.

In the southern part of the study area, the combination of σ_a and κ_a data over Amesbury 115 supports the presumed existence of a south-western entrance of the monument (Amadio and Bishop, 2010), as conductive anomalies suggest the presence of associated features adjoining the segmented ditch (Fig. 9b, G). Through validation of these anomalies and detailed analysis of the bedrock morphology, the presence of a south-eastern entrance for Amesbury 115 could be investigated further. In addition, the presence of the nearby palaeochannel segment could prove to have been instrumental in choosing the location of this monument.

5 Conclusions

The results presented here demonstrate how a wealth of information on the past and present soil variations at Stonehenge can be obtained through a single multi-receiver EMI survey. In addition, the methodology to remove the influence of topsoil metal on the EMI data overcame the masking effect of topsoil debris on sub-surface features. This provides a solution to outstanding issues in geophysical surveying within the Stonehenge landscape (Darvill et al. 2013, Gaffney et al. 2012), as this procedure can be implemented when using or interpreting other geophysical datasets. The multi-layered EMI dataset also enabled discriminating between different types of natural and anthropogenic soil variation within the study area. In this respect, the potential to identify the most significant data layers from this dataset, based on specific research questions, makes multi-receiver EMI a particularly versatile tool in geoarchaeological research. The mapped natural soil variability provides an insight into the palaeotopography of the area, which will facilitate the identification of potential archaeological and

palaeoenvironmental sampling locations. Modern soil disturbances were also identified, along with the remnants of flattened earthworks, showing how EMI can contribute to unveiling and managing the archaeology within the Stonehenge landscape. The simultaneous investigation of shallow and deeper soil layers through a multi-receiver EMI instrument has further allowed for the clearer delineation of archaeological features in the chalkland environment, and emphasises the value of discriminating between different soil volumes.

It has been proven that detailed geophysical soil mapping improves our knowledge of the Stonehenge environment, and offers an insight into the genesis of the current landscape. While invasive validation (e.g. coring) remains necessary, the results provide a robust basis for further geoarchaeological research. Through expanding this approach over a wider area, another significant step can be taken towards understanding the complex human-landscape interactions that have shaped the Stonehenge landscape.

6 Acknowledgements

The presented research was partly conducted in the framework of a post-doctoral research grant provided to Philippe De Smedt by the Research Foundation Flanders (FWO). The research was carried out in collaboration with the UK team of the Ludwig Boltzmann Institute for Archaeological Prospection and Virtual Archaeology (archpro.lbg.ac.at), which is based on an international cooperation of the Ludwig Boltzmann Gesellschaft (A), the University of Vienna (A), the Vienna University of Technology (A), ZAMG-the Austrian Central Institute for Meteorology and Geodynamic (A), the Province of Lower Austria (A), RGZM-the Roman-Germanic Central Museum Mainz (D), RAÄ-Swedish National Heritage Board (S), IBM VISTA-University of Birmingham (UK) and NIKU-Norwegian Institute for Cultural Heritage Research (N). We would like to thank the landowners of the area we surveyed, the National Trust. We would also like to thank Valentijn Van Parys for his invaluable contribution to the fieldwork.

7 References

Amadio, L., Bishop, S., 2010. *Stonehenge World Heritage Site Landscape Project. The Cursus Barrows & Surrounding Area* (English Heritage Archaeological Report 85), English Heritage, Portsmouth.

Bewley, R., Crutchley, S.P., Shell, C.A., 2005. New light on an ancient landscape; lidar survey in the Stonehenge World Heritage Site. *Antiquity* 79, 636-647.

Bonsall, J., Fry, R., Gaffney, C., Armit, I., Beck, A., Gaffney, V., 2013. Assessment of the CMD Mini-Explorer, a New Low-frequency Multi-coil Electromagnetic Device, for Archaeological Investigations. *Archaeological Prospection* 20, 219-231.

Canti, M., Campbell, G., Greaney, S., 2013. *Stonehenge, Wiltshire. Stonehenge World Heritage Site Synthesis: Prehistoric Landscape, Environment and Economy* (English Heritage Archaeological Report 45), English Heritage, Portsmouth.

Corwin, D.L., Lesch, S.M., 2005. Apparent soil electrical conductivity measurements in agriculture. *Computers and Electronics in Agriculture* 46, 11-43.

Crutchley, S.P., 2002. *Stonehenge Word Heritage Site Mapping Project* (English Heritage Aerial Survey Report Series 15), English Heritage, Swindon.

Darvill, T., 2006. *Stonehenge. The Biography of a Landscape.* Tempus Publishing Limited, Gloucestershire.

Darvill, T., Constant, V., Milner, E., Bender, B., Chan, B., Chandler, J., Crutchley, S., David, A., Field, D., Pearson, M.P., Ruggles, C., Woodward, A., 2005. *Stonehenge World Heritage Site: an Archaeological Research Framework*, English Heritage and Bournemounth University, London and Bournemouth.

Darvill, T., Lüth, F., Rassmann, K., Fischer, A., Winkelmann, K., 2013. Stonehenge, Wiltshire, UK: High Resolution Geophysical Surveys in the Surrounding Landscape, 2011. *European Journal of Archaeology* 16, 63-93.

De Smedt, P., Saey, T., Lehouck, A., Stichelbaut, B., Meerschman, E., Islam, M.M., Van De Vijver, E., Van Meirvenne, M., 2013a. Exploring the potential of multi-receiver EMI survey for geoarchaeological prospection: a 90 ha dataset. *Geoderma* 40, 1260–1267.

De Smedt, P., Saey, T., Meerschman, E., De Reu, J., De Clercq, W., Van Meirvenne, M., 2014. Comparing Apparent Magnetic Susceptibility Measurements of a Multi-receiver EMI Sensor to Topsoil and Profile Magnetic Susceptibility Data over Weak Magnetic Anomalies. *Archaeological Prospection* 21, 103-112.

De Smedt, P., Van Meirvenne, M., Davies, N.S., Bats, M., Saey, T., De Reu, J., Meerschman, E., Gelorini, V., Zwertvaegher, A., Antrop, M., Bourgeois, J., De Maeyer, P., Finke, P.A., Verniers, J., Crombé, P., 2013b. A multidisciplinary approach to reconstructing Late Glacial and Early Holocene landscapes. *Journal of Archaeological Science* 40, 1260-1267.

De Smedt, P., Van Meirvenne, M., Herremans, D., De Reu, J., Saey, T., Meerschman, E., Crombé, P., De Clercq, W., 2013c. The 3-D reconstruction of medieval wetland reclamation through electromagnetic induction survey. *Scientific Reports* 3, 1-5.

French, C., 2003. *Geoarchaeology in Action. Studies in soil micromorphology and landscape evolution*. Routledge, New York.

Gaffney, C., Gaffney, V., Neubauer, W., Baldwin, E., Chapman, H., Garwood, P., Moulden, H., Sparrow, T., Bates, R., Löcker, K., Hinterleitner, A., Trinks, I., Nau, E., Zitz, T., Floery, S., Verhoeven, G., Doneus, M., 2012. The Stonehenge Hidden Landscapes Project. *Archaeological Prospection* 19, 147-155.

Goovaerts, P., 1997. *Geostatistics for natural resources evaluation*. Applied Geostatistics Series. Oxford University Press, New York, USA.

Hopson, P.M., Farrant, A.R., Newell, A.J., Marks, R.J., Booth, K.A., Bateson, L.B., Woods, M.A., Wilkinson, I.P., Brayson, J., Evans, D.J., 2006. *Geology of the Salisbury Sheet Area*, Natural Environment Research Council, Nottingham.

ICOMOS, 1986. *World Heritage List n° 373*, International Council on Monuments and Sites, Paris.

Leivers, M., Moore, C., 2008. *Archaeology on the A303 Stonehenge Improvement*. Trust for Wessex Archaeology Ltd.

Macphail, R.I., Crowther, J., 2008. Appendix 1: Soil. In: M. Leivers, C. Moore (Eds.), *Archaeology on the A303 Stonehenge Improvement*. Wessex Archaeology, Wessex, pp. 1-24.

McNeill, J.D., 1980. *Electromagnetic terrain conductivity measurement at low induction numbers*. Technical Note 6, Geonics Limited, Ontario.

Quinault, C., 2012. *Green waste contamination fears raised by MP*. Available: http://www.letsrecycle.com/news/latest-news/compost/mp-raises-concerns-over-compost-contamination (last accessed: 14/01/2014).

Rhoades, J.D., Raats, P.A.C., Prather, R.J., 1976. Effects of Liquid-phase Electrical Conductivity, Water Content, and Surface Conductivity on Bul.k Soil Electrical Conductivity. *Soil Science Society of America Journal* 40, 651-655.

Richards, J., 1990. *The Stonehenge Environs Project*. (English Heritage Archaeogical Report 16). Hobbs the Printers of Southampton, Southampton.

Rossel, V., McBratney, A.B., Budiman, M. (Eds.), 2010. *Proximal Soil Sensing*. Progress in Soil Science. Springer.

Saey, T., Simpson, D., Vermeersch, H., Cockx, L., Van Meirvenne, M., 2009b. Comparing the EM38DD and Dualem-21S sensors for depth-to-clay mapping. *Soil Science Society of America Journal* 73, 7-12.

Saey, T., Simpson, D., Vitharana, U.W.A., Vermeersch, H., Vermang, J., Van Meirvenne, M., 2008. Reconstrucing the paleotopography beneath the loess cover with the aid of an electromagnetic induction sensor. *Catena* 74, 58-64.

Saey, T., Van Meirvenne, M., Vermeersch, H., Ameloot, N., Cockx, L., 2009a. A pedotransfer function to evaluate the soil profile textural heterogeneity using proximally sensed apparent electrical conductivity. *Geoderma* 150: 389-395.

Scollar, I., Tabbag, A., Hesse, A. and Herzog, I. 1990., *Archaeological Prospecting and Remote Sensing*. Topics in Remote Sensing. Cambridge University Press, Cambridge.

Simpson, D., Van Meirvenne, M., Lück, E., Rühlmann, J., Saey, T., Bourgeois, J., 2010. Sensitivity of multi-coil frequency domain electromagnetic induction sensors to map soil magnetic susceptibility. *European Journal of Soil Science* 61, 469-478.

Simpson, D., Van Meirvenne, M., Saey, T., Vermeersch, H., Bourgeois, J., Lehouck, A., Cockx, L., Vitharana, U.W.A., 2009. Evaluating the multiple coil configurations of the EM38DD and DUALEM-21S sensors to detect archaeological anomalies. *Archaeological Prospection* 16, 91-102.

Slavich, P., Petterson, G., 1990. Estimating average rootzone salinity from electromagnetic induction (EM-38) measurements. *Australian Journal of Soil Research* 28, 453-463.

Sudduth, K.A., Kitchen, N.R., Wiebold, W.J., Batchelor, W.D., Bollero, G.A., Bullock, D.G., Clay, D.E., Palm, H.L., Pierce, F.J., Schuler, R.T., Thelen, K.D., 2005. Relating apparent electrical conductivity to soil properties across the north-central USA. *Computers and Electronics in Agriculture* 46, 263-283.

Underhill, W., 2011. Putting Stonehenge in its place. *Scientific American* 304, 48-53.

Wait, J.R., 1962. A note on the electromagnetic response of a stratified earth. *Geophysics* 27, 382-385.

8 Figure captions

Figure 1: Satellite image of the core of the Stonehenge World Heritage Site (source: Google Earth, © 2010 Google) with indication of the 22 ha EMI survey area (A), the extent of the Stonehenge Cursus (B) and the Stonehenge monument (C).

Figure 2: **a**) σ_a data from the 1 m HCP coil configuration showing numerous negative anomalies related to metallic topsoil debris, **b**) location of the metallic topsoil debris based on the 1 m HCP σ_a data (Coordinates in meters UTM 30N, WGS 84). The arrows in (**a**) indicate the anomalies shown in Fig. 3 (arrow 1), and Fig. 4 (arrow 2)

Figure 3: Comparison of the influence of a metal-induced anomaly on the EMI measurements. The position of the transect is shown over the 1 m HCP σ_a data (**a**) and κ_a data (**b**) plots. In (**c**) the σ_a data from each coil configuration are compared along this transect, **d**) shows the κ_a data from the 1 m and 2 m HCP coil pairs along the transect. The location of the anomaly is indicated on Fig. 2a (arrow 1).

Figure 4: Comparison of metal influence removal in the 2 m HCP κ_a data with and without the 1 m filter buffer. The left column shows the interpolated data, while the column on the right shows the individual data points. In **a**), the original anomaly is shown in the 2 m HCP κ_a data. The filtered 2 m HCP κ_a data without (**b**) and with (**c**) implementation of a 1 m filter buffer are shown below. The location of the anomaly is indicated on Fig. 2a (arrow 2), and on Fig. 5 (arrow 2).

Figure 5: Comparison of the anomalies detected at the hengiform monument (see Gaffney et al. 2012) as seen in the 2 m HCP κ_a data before (**a**) and after (**b**) metal removal. In (**a**), two anomalies are indicated that were related to the metal topsoil debris, in (**b**) a group of anomalies are indicated that remained present in the filtered data, which suggest the presence of pits.

Figure 6: The 2 m PRP σ_a data, representative for the soil variation between 0 m – 1 m below the sensor (**a**). The variation shows a central chalk ridge (A) bordered by more conductive soil in the north and south. In the north two circular anomalies are indicated (B) that are related to grassland fungi. In (**b**) the 1 m HCP κ_a data are shown, revealing possible palaeochannel deposits in the south of the area (C). Further magnetic anomalies include large linear features within the boundaries of the Cursus (D), and two circular anomalies that possibly indicate ploughed barrow monuments (E).

Figure 7: The 1 m PRP σ_a data (**a**), and the 2 m HCP κ_a data (**b**) with a detail of the small causewayed ditch (Amesbury 115) shown in (**c**). In (**a**), apart from the Cursus ditches in the north of the area the different barrow monuments can clearly be discriminated in the centre of the field. Small conductive anomalies that could be related to archaeology are found in the south of the field (A), and within the Cursus boundaries (e.g. B). In (**b**), the most characteristic κ_a-anomalies are; the pit-like anomalies (C) and the linear features (D) detected inside the Cursus monument, the annular and round anomalies related to barrow monument Amesbury 49 (E), two traces of possible ploughed barrows aligned between the known monuments (G) and the hengiform monument (F) located at the site of Amesbury 50.

Figure 8: Modern soil disturbance and metal contamination within the survey area based on the EMI data.

Figure 9: a) Soil map derived from the σ_a data with indication of the palaeochannel (black dashed line) attested in the κ_a data, and plotted elevation contours (elevation in meters WGS 84). **b**) Overview of the detected geoarchaeological variability, showing the soil variation and the location of the most characteristic anomalies indicating archaeology. These include; known barrow monuments Amesbury 48 (A) and 49 (B), two possible ploughed barrow monuments (C), the Cursus ditches and adjacent banks (D), pits (E) and linear anomalies (F) inside the Cursus, a causewayed ditch and adjoining anomalies near the south-west of the structure (G), several small ditch-like anomalies (H), the hengiform monument at Amesbury 50 (I).

Figure 1

Click here to download high resolution image

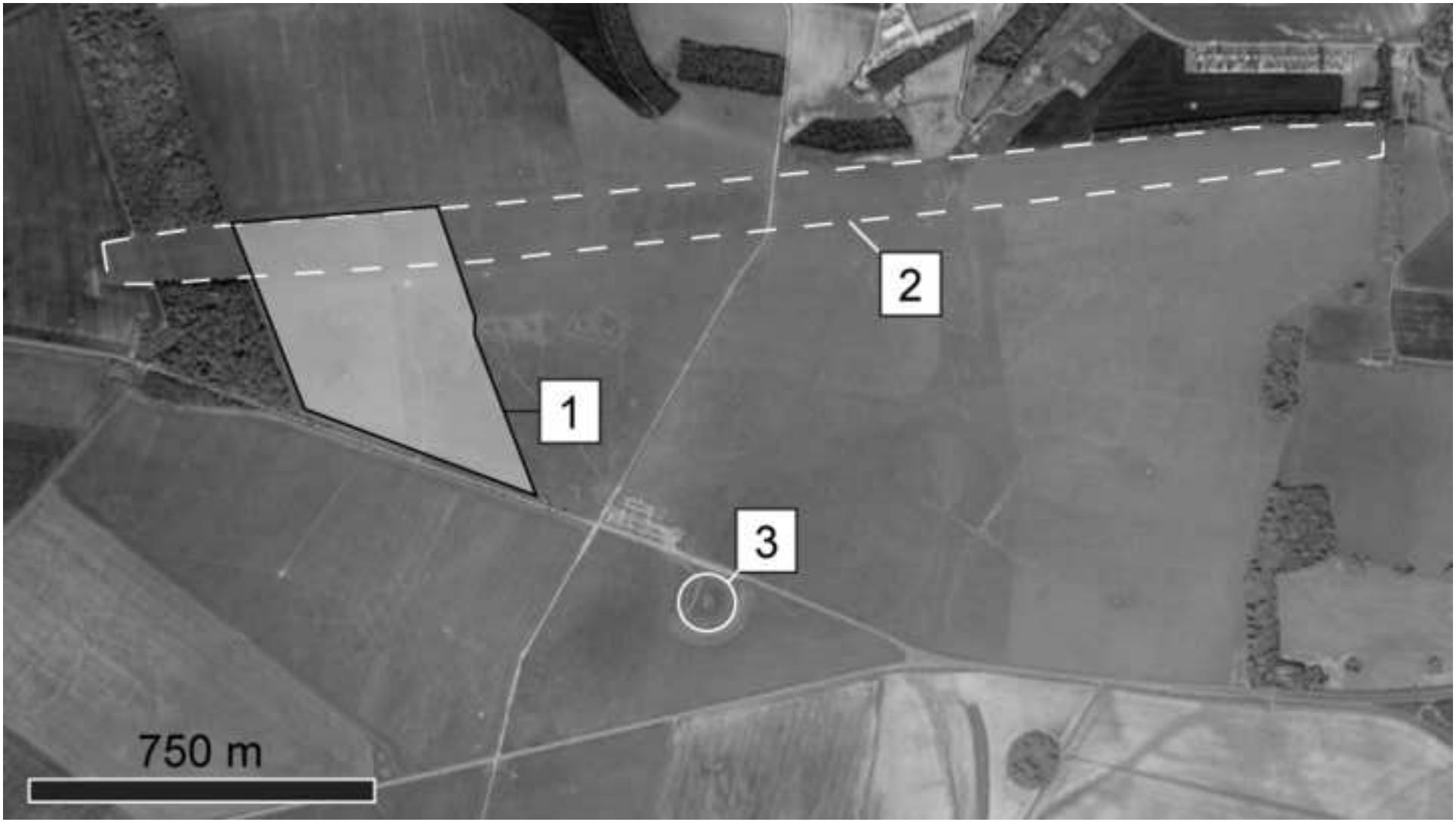

Figure 2

Click here to download high resolution image

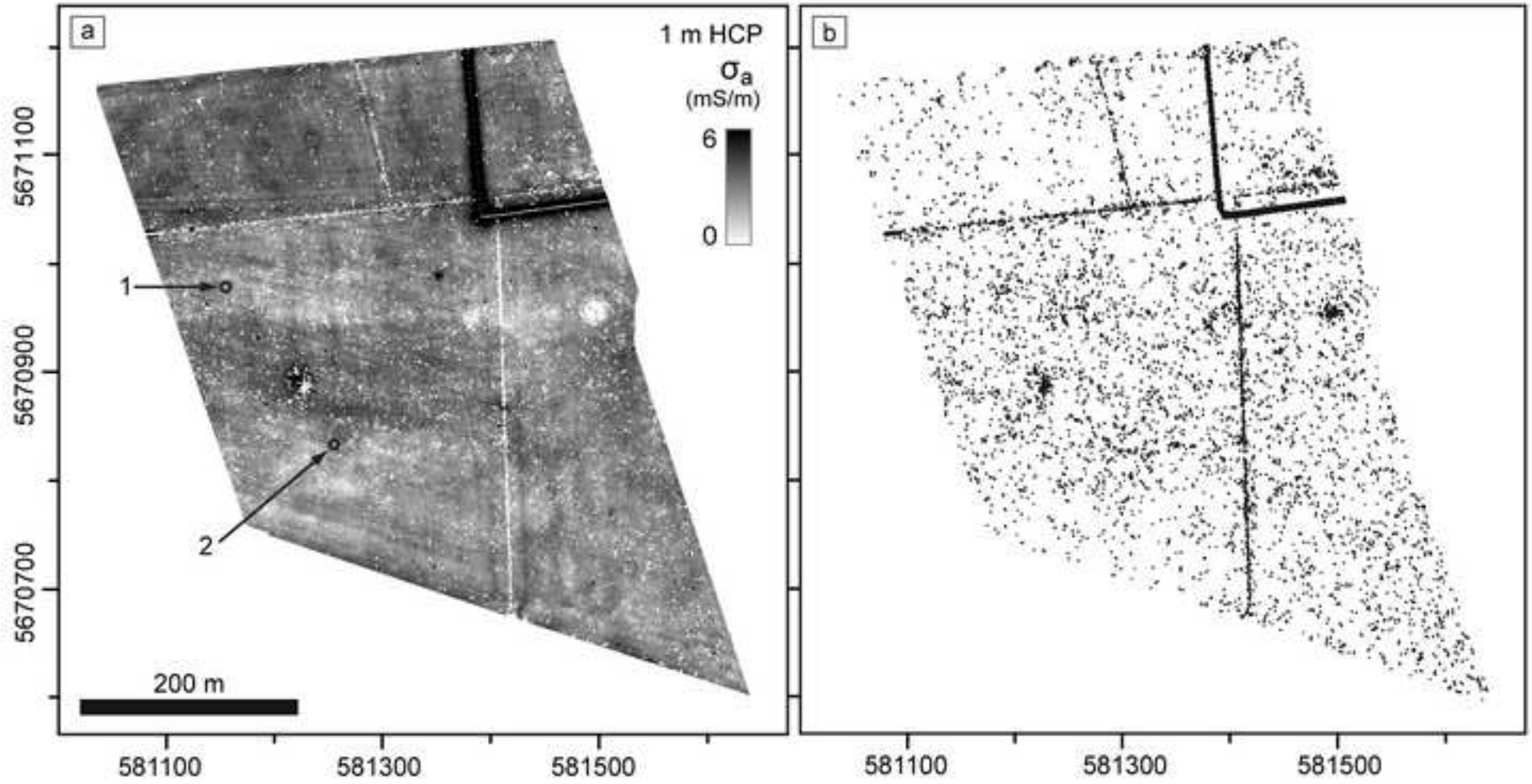

Figure 3

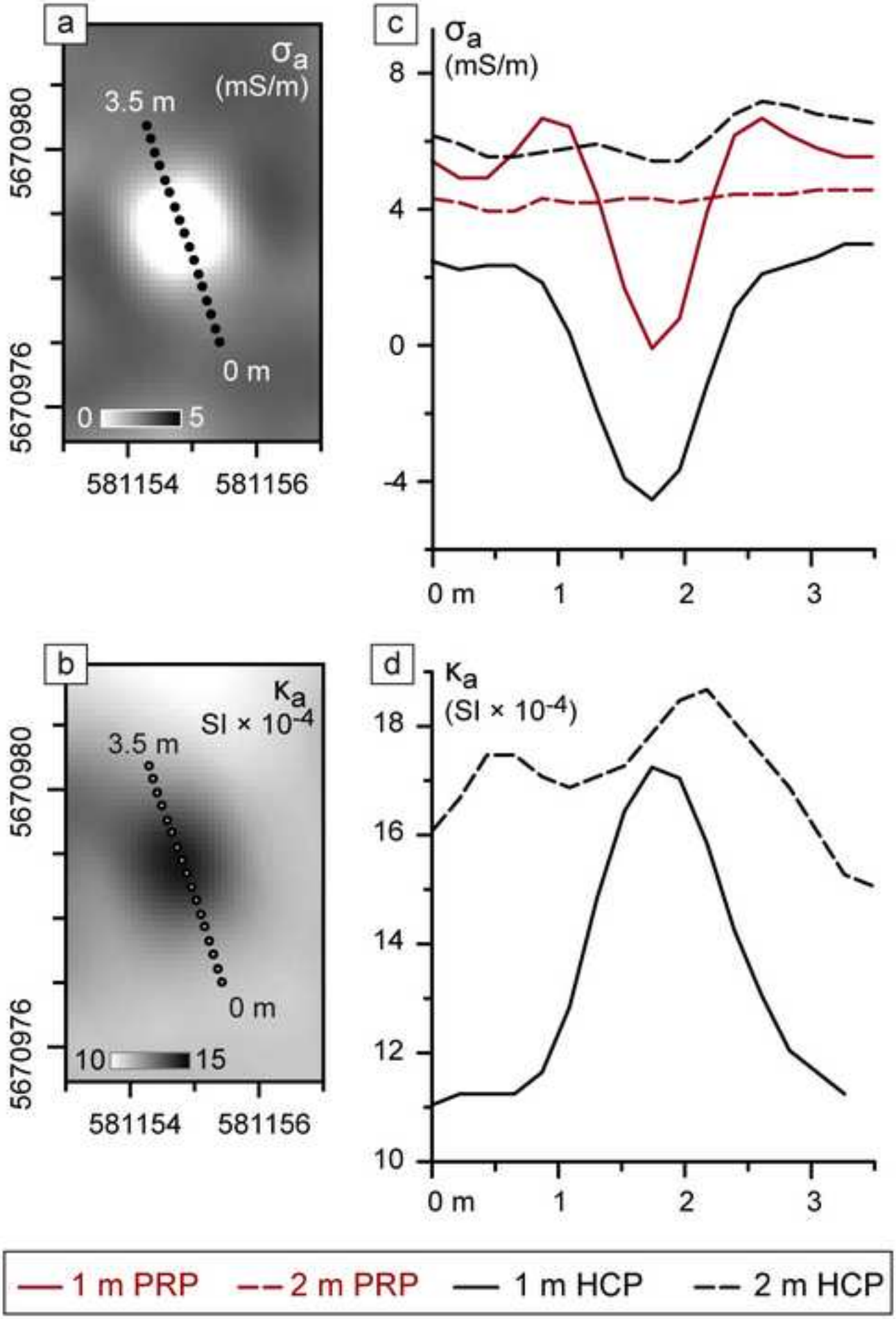

Figure 4

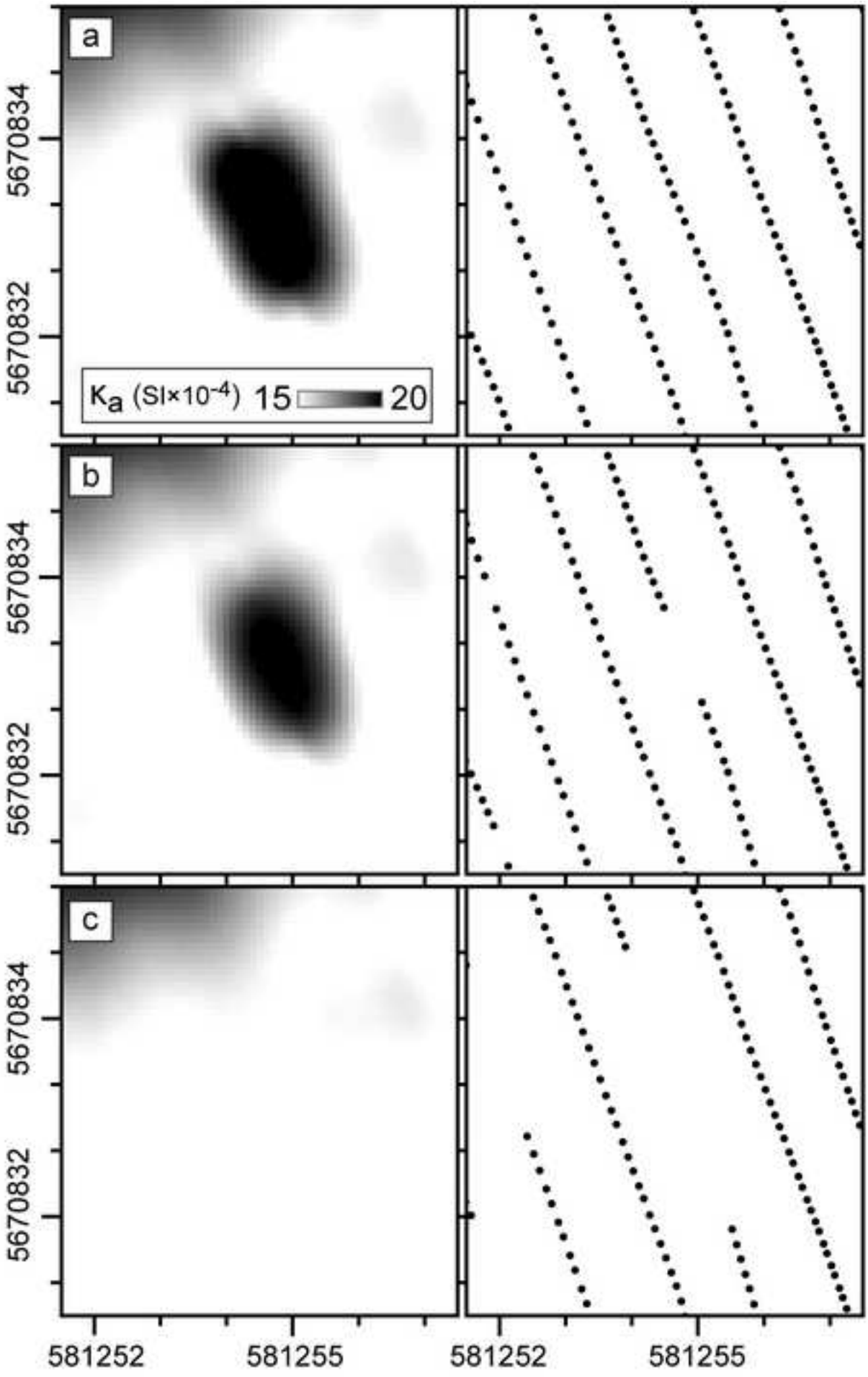

Figure 5

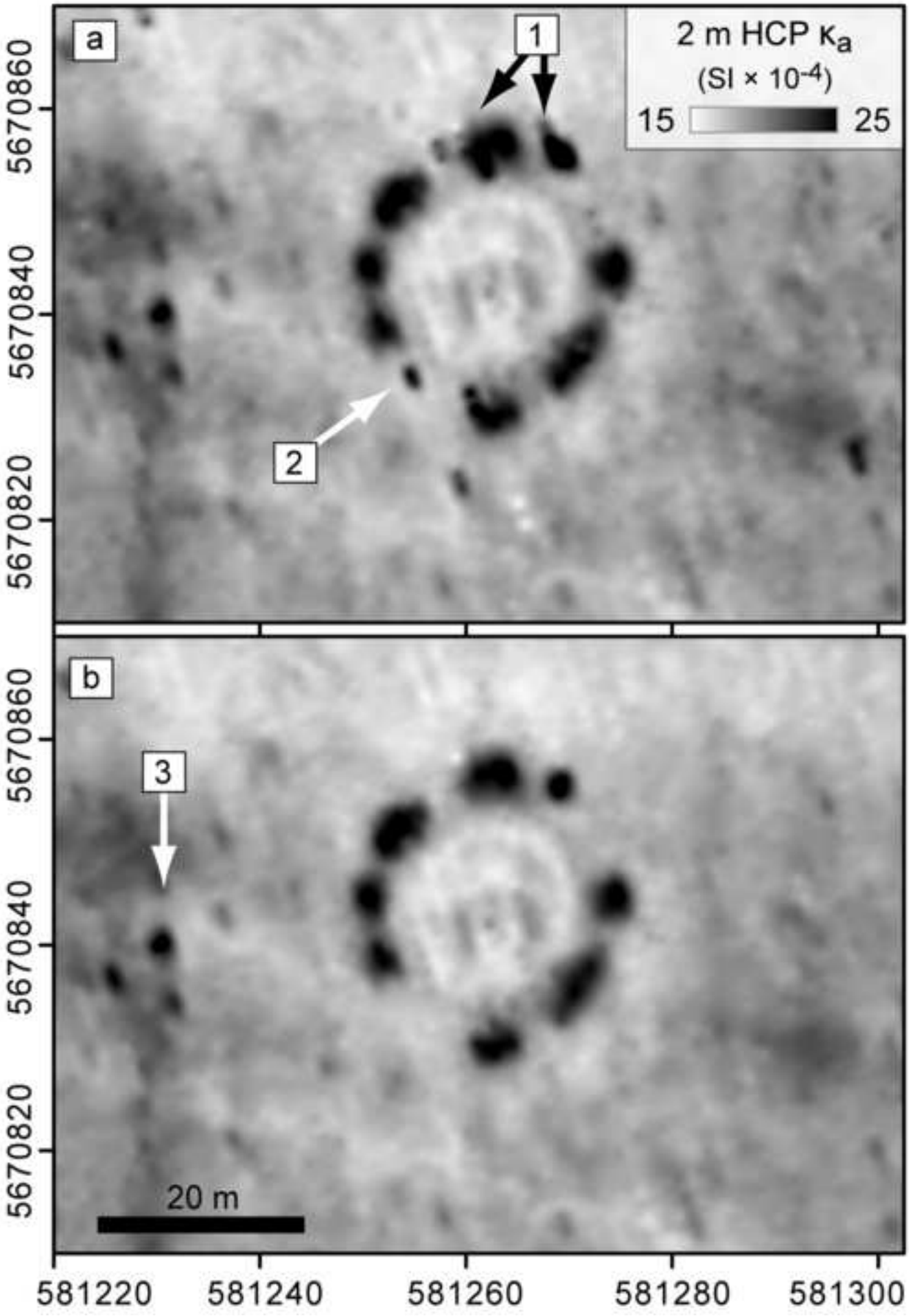

Figure 6

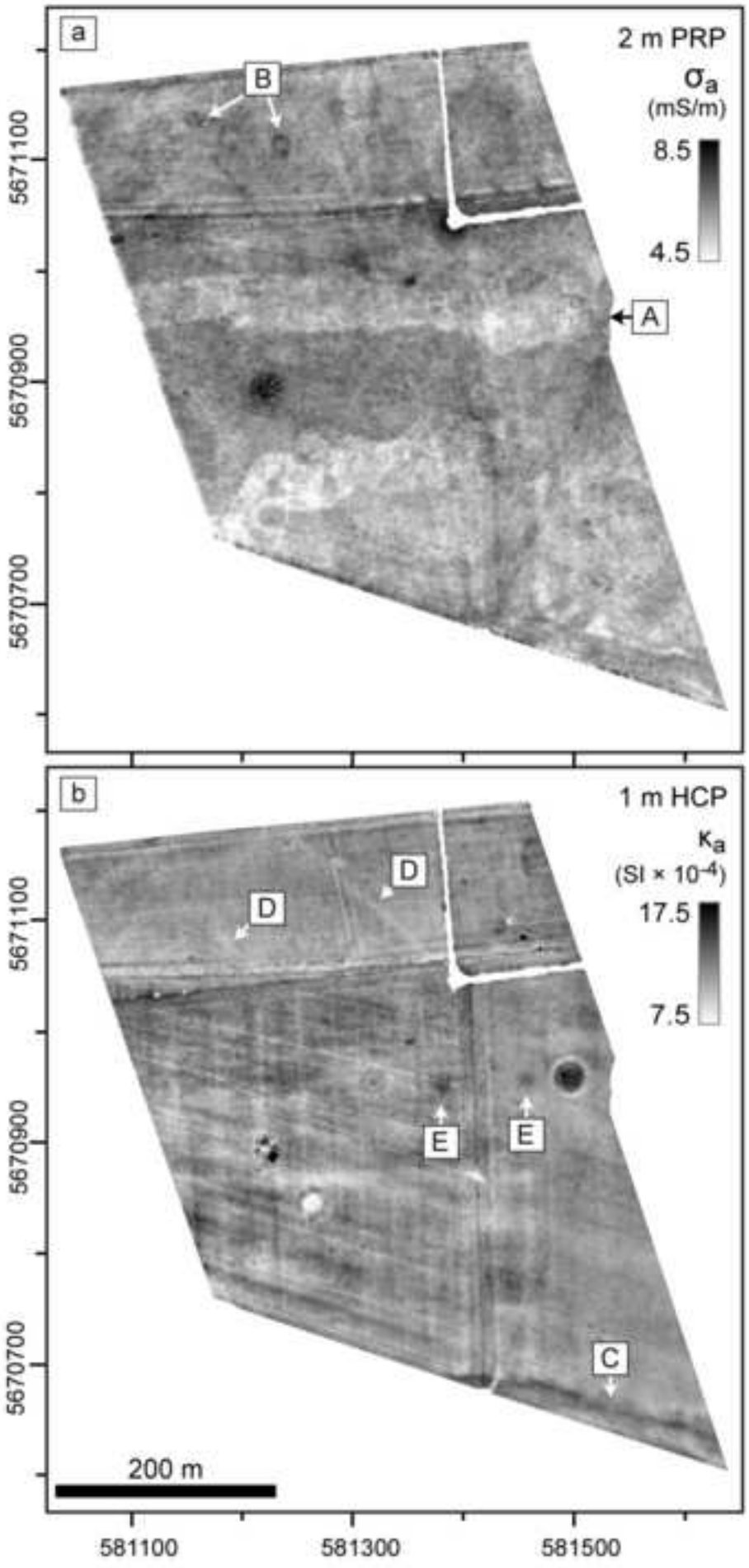

Figure 7
Click here to download high resolution image

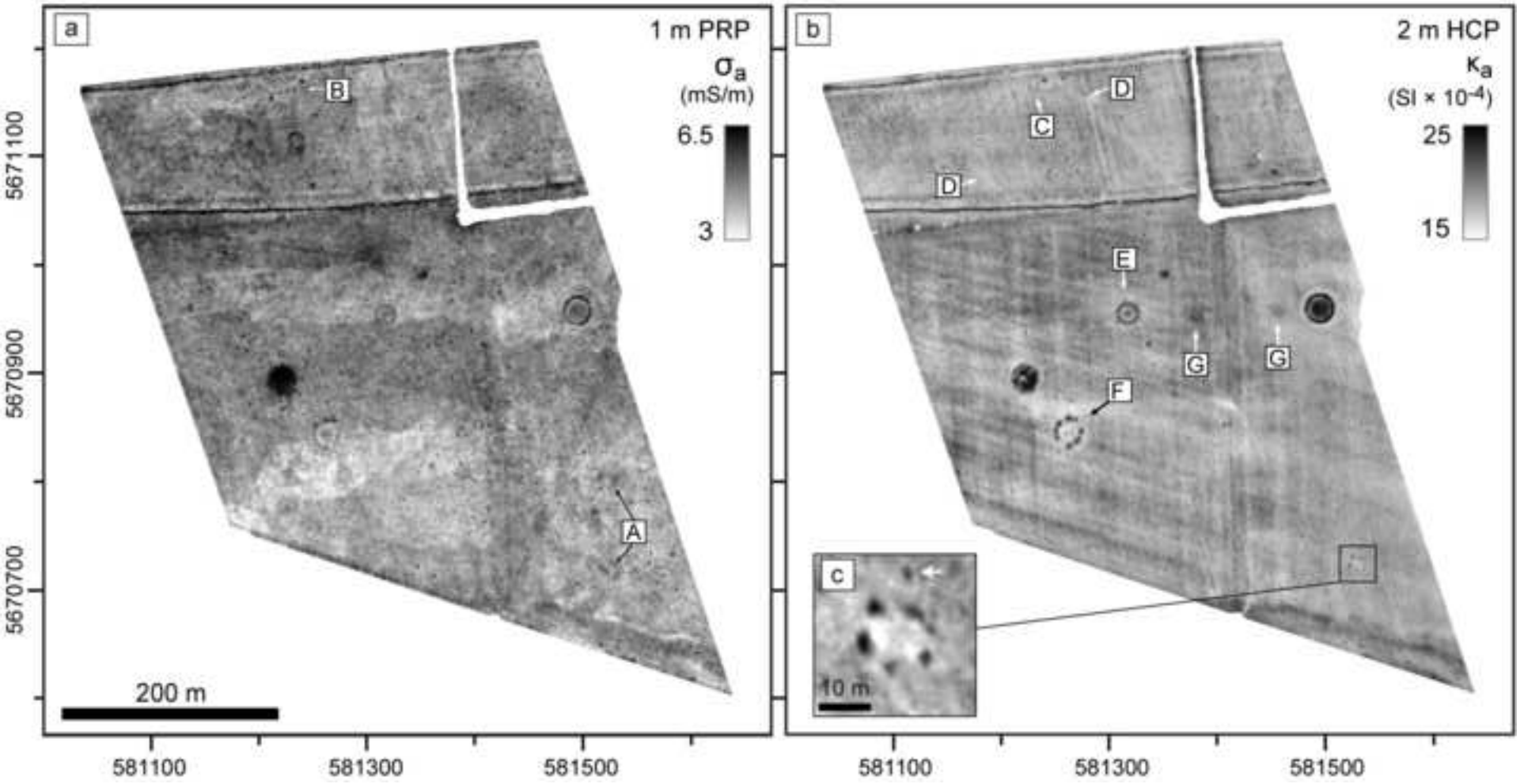

Figure 8

Click here to download high resolution image

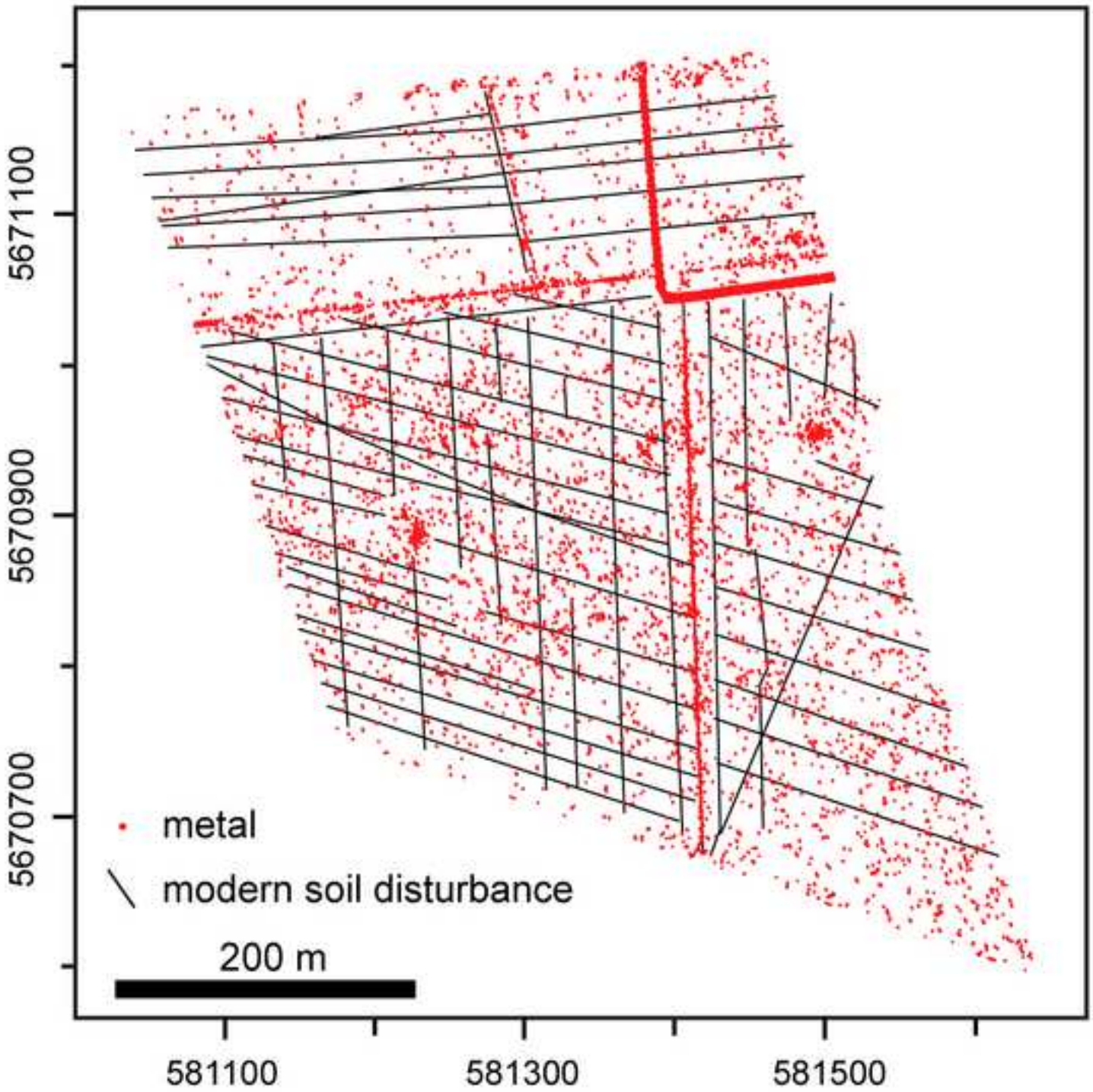

Figure 9

Click here to download high resolution image